Simulations of High Resolution Electron Microscopy Images of Icosahedral Quasicrystals

Marianne Quiquandon, Denis Gratias, Jean-Tristan Beauchesne

Simulations of High Resolution Electron Microscopy Images of Icosahedral Quasicrystals

Journal:	*Philosophical Magazine & Philosophical Magazine Letters*
Manuscript ID:	TPHM-07-Nov-0319.R1
Journal Selection:	Philosophical Magazine
Date Submitted by the Author:	08-Jan-2008
Complete List of Authors:	Quiquandon, Marianne; CNRS/ONERA, LEM Gratias, Denis; CNRS/ONERA, LEM Beauchesne, Jean-Tristan; CNRS/ONERA, LEM
Keywords:	HREM, quasicrystalline alloys, simulation
Keywords (user supplied):	HREM, quasicrystalline alloys, simulation
Note: The following files were submitted by the author for peer review, but cannot be converted to PDF. You must view these files (e.g. movies) online.	
Quiquandonetal.tex	

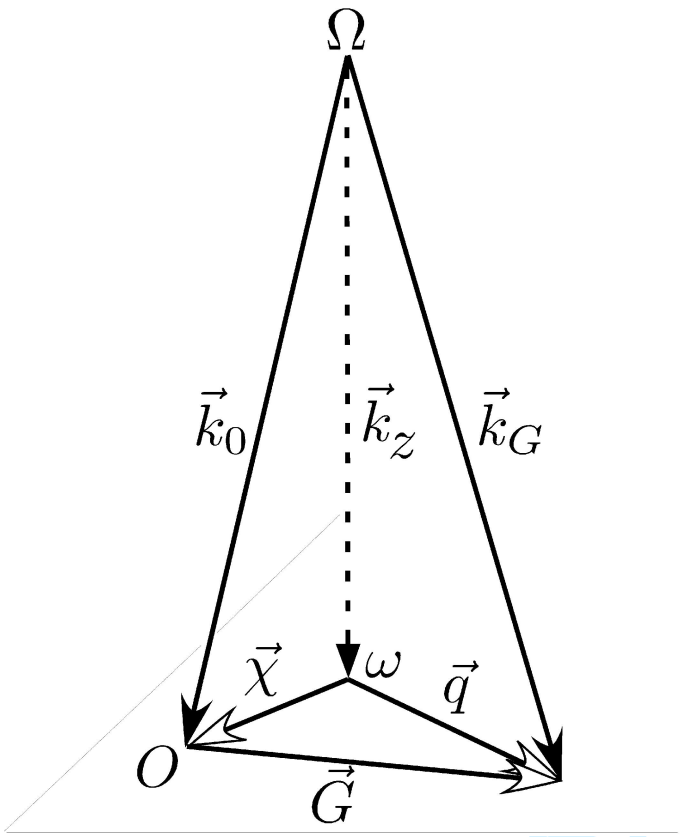

(a)

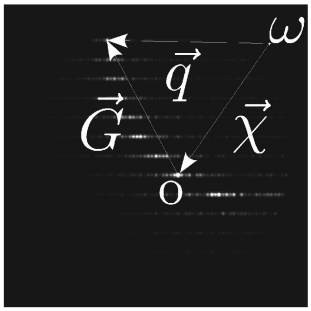

(b)

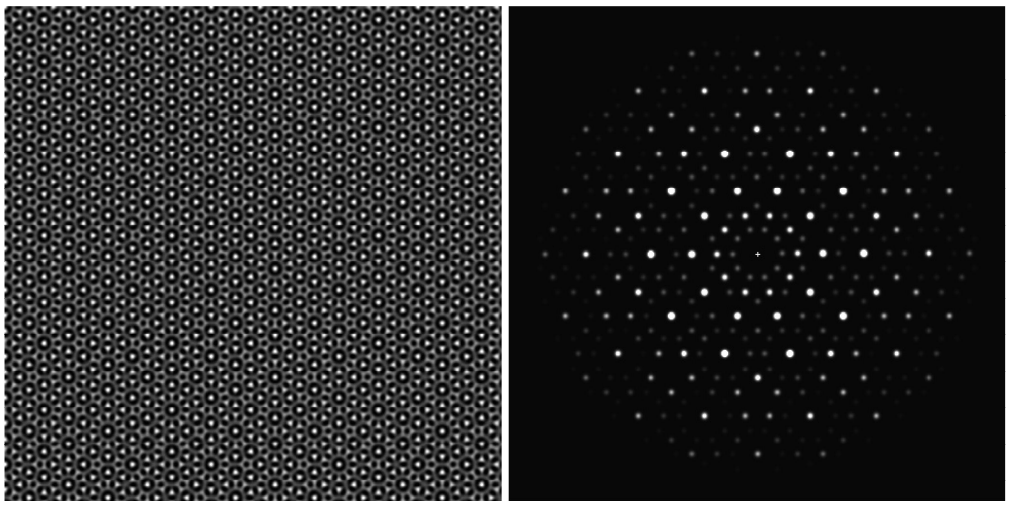

Unable to Convert Image

The dimensions of this image (in pixels) are too large to be converted. For this image to convert, the total number of pixels (height x width) must be less than 40,000,000 (40 megapixels).

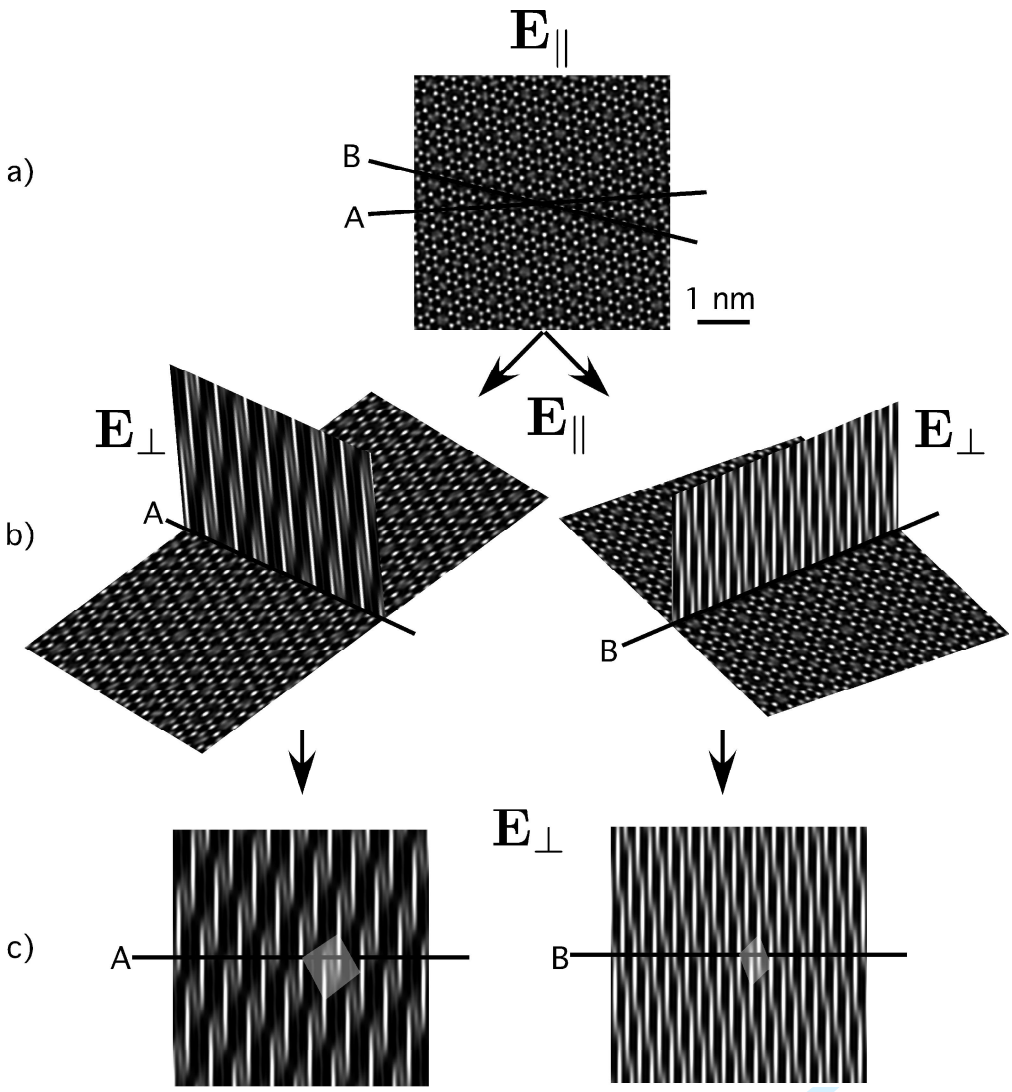
a)
$\mathbf{E}_{\parallel}$
B
A
1 nm
b)
$\mathbf{E}_{\perp}$
A
$\mathbf{E}_{\parallel}$
$\mathbf{E}_{\perp}$
B
c)
A
$\mathbf{E}_{\perp}$
B

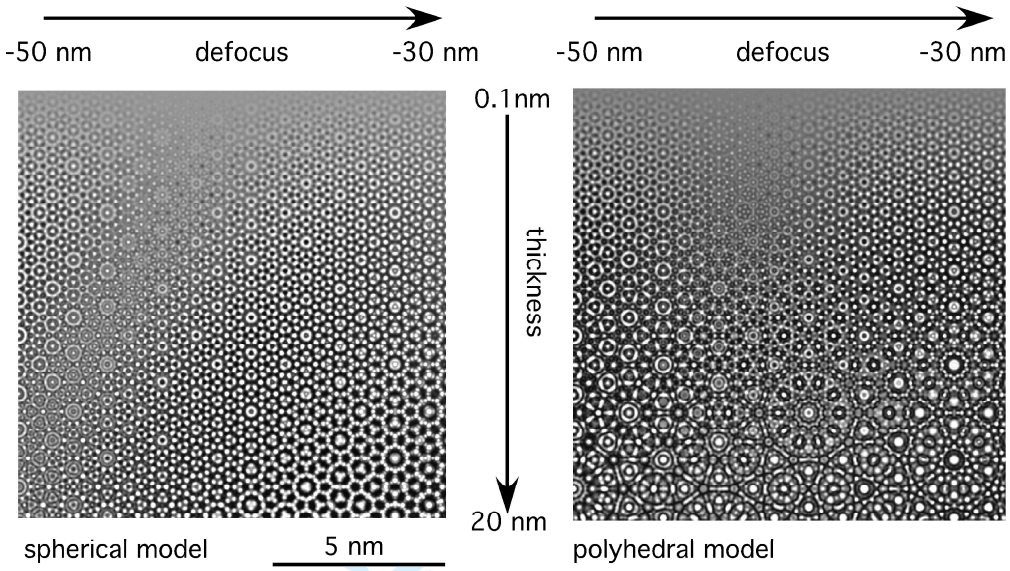

Philosophical Magazine,
Vol. 00, No. 00, DD Month 200x, 1–7

Simulations of High Resolution Electron Microscopy Images of Icosahedral Quasicrystals

Marianne Quiquandon, Jean-Tristan Beauchesne and Denis Gratias
LEM-CNRS/ONERA, B.P. 72
92322 Châtillon cedex, France

(Received 00 Month 200x; in final form 00 Month 200x)

We apply the scattering matrix formulation for calculating the images of high resolution electron microscopy (HREM) images of quasiperiodic crystals and discuss their basic properties. The main feature in the image formation comes from the truncation effects of the q-basis, especially the perpendicular components that must be numerous enough for properly reproducing quasiperiodicity. A comparison between two types of atomic structural model is presented that illustrate the difficulties of differentiating the models from the HREM observations.

1 Introduction

Electron microscopy has been the main tool in the discovery of quasicrystals: dark field images [1, 2] and High Resolution Electron Microscopy pictures (HREM) [3, 4] have given the most convincing experimental proofs that icosahedral quasicrystals exist. Image simulations in dynamical diffraction took some more time to emerge once it has been formalised that there was no basic difficulty to deal with quasiperiodicity instead of periodicity as demonstrated by M. Cornier *et al.* [5–8] for the matrix formulation and T. Watanabe and Y. Kitano [9] for the multislice technique (see also W. Yuan-Ming *et al.* [10] for another analysis based on the multislice method).

This paper reports a detailed quantitative study of the computation of dynamical electron diffraction of quasicrystals and HREM images and draws some conclusions of what can be really extracted from HREM images with respect to the problem of atomic structure determination.

1.1 *Dynamical electron diffraction*

Dynamical elastic diffraction of fast electrons can be described in a good approximation as a Schrödinger-like equation [11–16] of a 2D object moving along the propagation direction z of the electrons, that can be assimilated to a parameter. We shall make the usual assumption that the thickness of the sample is small and the variation along z of the potential is smooth enough for the potential being well approximated by the z average projected potential[1]. Under these all conditions, the diffraction Hamiltonian is explicitly written as:

$$\widehat{\mathbf{H}} = \frac{1}{2k_z}\Big(\sum_q |q\rangle(q^2-\chi^2)\langle q| + \sum_{q,q'} |q\rangle\langle q|\bar{V}|q'\rangle\langle q'|\Big) \tag{1}$$

where $\chi^2 = k_0^2 - k_z^2$ and $\bar{V}$ is the projected potential. As shown in fig 1, the 3D dynamical variables $\vec{r}$ and $\vec{k}$ are decomposed in their components on the image and diffraction planes, respectively $\vec{\rho}$ and $\vec{q}$, and on the

[1]The projected potential approximation requires carefull examination in the case of quasicrystals. It turns out that representing the propagation direction in the 2D plane of the high dimension space shows that the 2D cell in that plane has sizes of the same order of magnitude than in crystals and the potential fluctuates in a similar fashion thus making this approximation equivalent in crystals and quasicrystals.

Philosophical Magazine
ISSN 1478-6435 print/ISSN 1478-6443 online
http://www.tandf.co.uk/journals
DOI: 10.1080/1478643YYxxxxxxxx

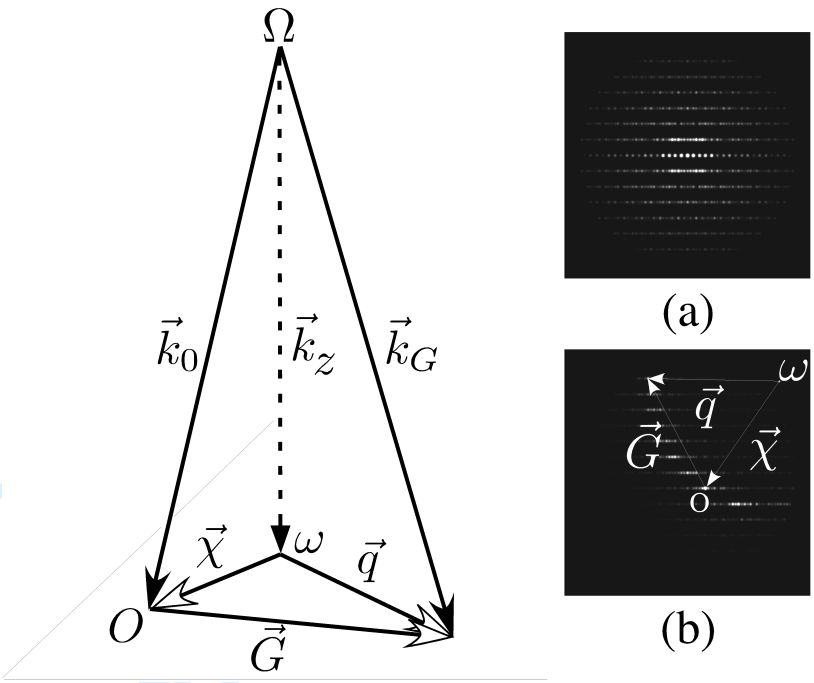

Figure 1. Definition of the geometry of fast electron diffraction. The incident beam with wavevector $\vec{k}_0$ is diffracted in the direction $\vec{k}_G$. The initial wavevector decomposes along the z direction perpendicular to the diffraction plane according to $\vec{k}_0 = \vec{k}_z + \vec{\chi}$ and the diffracted wavevector $\vec{k}_G = \vec{k}_z + \vec{q}$. The center Ω of the Ewald sphere projects at the point ω in the diffraction plane. The origin of the reciprocal lattice is located at the extremity of $\vec{\chi}$ with origin ω, so that $\vec{q} = \vec{\chi} + \vec{G}$ where $\vec{G}$ is a vector of the reciprocal lattice. The inserts (a) and (b) show typical simulations of diffraction patterns of usual crystals; the exact Laue symmetric position shown in (a) is characterized by $\vec{\chi} = 0$ and therefore $\vec{q} = \vec{G}$.

perpendicular directions, respectively z and k_z. The initial state at $z = 0$, is the plane wave $|\chi\rangle$. The state $|\Psi(z)\rangle$ at thickness $z > 0$ is given by $|\Psi(z)\rangle = \sum_j |j\rangle e^{-iE_j z}\langle j|\chi\rangle$ where $|j\rangle$ and E_j are the eigenvectors and eigenvalues of the Hamiltonian $\widehat{\mathbf{H}}$. The diffraction intensity $I_q(z)$ in the q direction, and the image $I_\rho(z)$ at location ρ, both at thickness z are given by:

$$\langle q|\Psi(z)\rangle = \sum_j \langle q|j\rangle e^{-iE_j z}\langle j|\chi\rangle, \quad I_q(z) = |\langle q|\Psi(z)\rangle|^2 \tag{2}$$

$$\langle \rho|\Psi(z)\rangle = \sum_q \sum_j \langle \rho|q\rangle \widehat{\mathbf{T}}(q)\langle q|j\rangle e^{-iE_j z}\langle j|\chi\rangle, \quad I_\rho(z) = |\langle \rho|\Psi(z)\rangle|^2 \tag{3}$$

where $\widehat{\mathbf{T}}(q)$ is the optical transfer function (see for instance [20,21] for a detailed description of the transfer function).

1.2 *Diffraction of quasiperiodic objects*

The only condition imposed by equation (1) is that the set $\{\vec{q}\}$ of the wavevectors be an *enumerable* set such that the Hamiltonian can be written as a matrix with a *finite* number of rows and columns (limited by an arbitrary cut off the $\{\vec{q}\}$ basis at large $\vec{q}$). This is trivially fulfilled for crystals because the scattering potential has a *lattice* as Fourier carrier thus distributes on discrete Bragg peaks. This is also fulfilled for quasicrystals since there, the potential has a $\mathbb{Z}$*-module* as Fourier carrier that is again an *enumerable* set of Bragg peaks. *There is therefore no need of artificially introducing large crystalline supercells* (see [5–8]). The off-diagonal elements of $\widehat{\mathbf{H}}$ are proportional to the structure factors as computed from the cut method[1].

[1]The atomic model is generated by a cut along the 3D physical space noted $\mathbf{E}_\parallel$ of a periodic structure in a large hyperspace of dimension N; this structure is defined by a collection of bounded polytopes, here volumes, called "atomic surfaces" aligned along the subspace $\mathbf{E}_\perp$

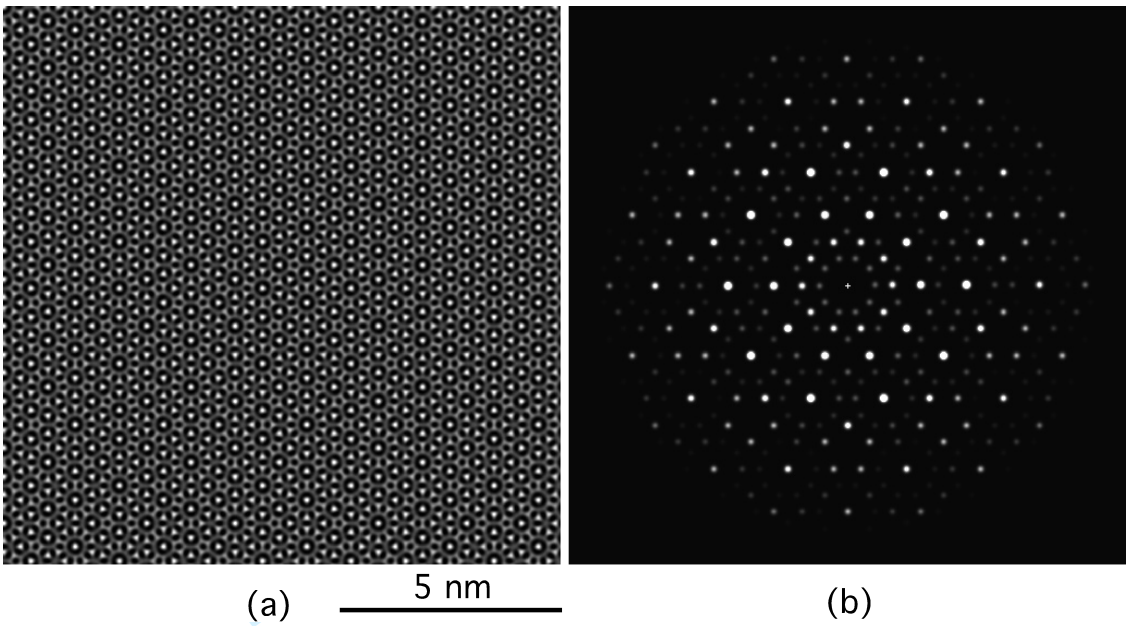

Figure 2. (a) Simulation along the 5-fold direction of a HREM image of the i-AlPdMn phase with the structural model described in [17]. The computation is performed at 200 keV using 461 beams shown on the calculated diffraction pattern (b). The thickness of the foil is $z = 5$ nm, at a defocus of $\Delta z = -50$ nm, with the optical aberration parameters $C_s = 1$ mm, $\alpha = 0.1$ mrad and $C_c = 4$ mm.

Considering two N-dimensional wavevectors $\vec{q}$ and $\vec{q'}$ and introducing $\vec{Q} = \vec{q} - \vec{q'}$ that decomposes along respectively $\mathbf{E}_\parallel$ and $\mathbf{E}_\perp$ according to $\vec{Q} = \vec{Q}_\parallel + \vec{Q}_\perp$, we can compute the structure factor explicitly using:

$$\langle q|\bar{V}|q'\rangle = \hat{V}(\vec{Q}) = \frac{1}{\Omega}\sum_{j=1}^{K} f_j(\vec{Q}_\parallel)\chi_k(\vec{Q}_\perp)e^{2i\pi\vec{Q}.\vec{R}_j}$$

where Ω is the (hyper)volume of the unit cell in the hyperspace, K is the number of the different atomic surfaces (or acceptance windows) in the perpendicular space $\mathbf{E}_\perp$ located at sites $\vec{R}_j$ in the hyperspace, $\chi_k(\vec{Q}_\perp)$ their Fourier transform for the argument $\vec{Q}_\perp$ and $f_j(\vec{Q}_\parallel)$ the corresponding form factors for the atomic species associated to the j-th atomic surface.

The potentials are calculated for i-AlPdMn using both a polyhedral model recently proposed by the present authors [17] and the spherical model of Boudard et al. [18] that has the main advantage of leading to very short computation time. As an example, fig 2 shows a numerical HREM simulation observed along a 5-fold direction; it is built with 461 excited beams of the quasiperiodic 6D-lattice, it has no periodicity and shows the usual properties of quasiperiodicity.

2 Diffracted amplitudes and images of quasicrystals

2.1 *Evolution of the beam intensities as a function of the size of the q-basis*

The main problem in computing the eigenstates of the Hamiltonian (1) is the numerical stabilization of the values when increasing the size of the q-basis. It is different from crystals because, here the q-basis (see [8]) is dense. The intensity of the central beam versus thickness is reported on fig 3 for various q-bases of increasing size using the spherical model made of pure aluminum:

- on the left part of the figure, the q-basis is built with 6D Q vectors with perpendicular components $|Q_\perp|$ bounded by $2 + 3\tau$ and parallel components $|Q_\parallel|$ increasing from $3 + 5\tau$ to $13 + 21\tau$;

perpendicular to $\mathbf{E}_\parallel$.

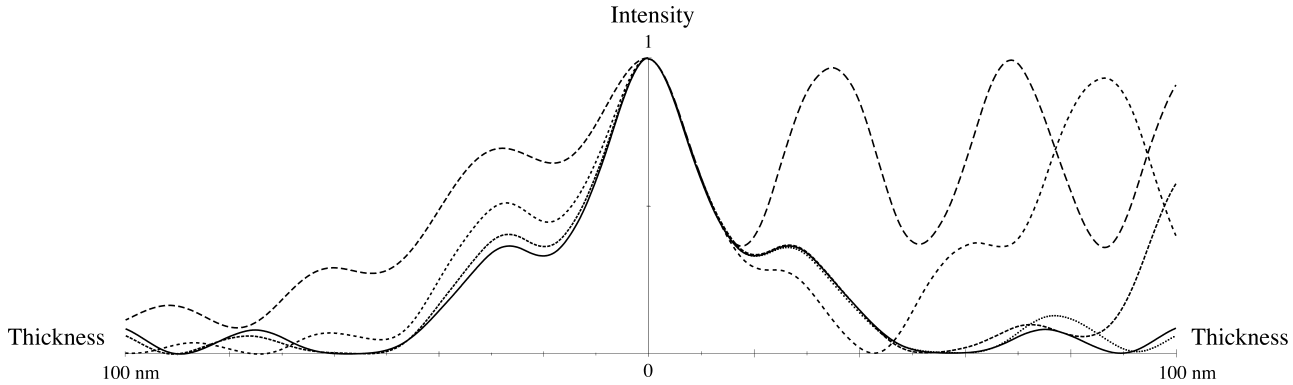

Figure 3. Intensity of central beam versus thickness for various q-bases. On the left the max $|Q_\perp|$ value is fixed to $2+3\tau$ with increasing $|Q_\parallel|$ values from $3+5\tau$ (large dash) to $13+21\tau$ (finer dashes to continuous line). On the right, the max $|Q_\parallel|$ value is fixed to $13+21\tau$ with increasing $|Q_\perp|$ values from 1 to $2+3\tau$.

- on the right part, the q-basis is limited to 6D Q vectors with parallel components $|Q_\parallel|$ bounded by $13+21\tau$ and perpendicular components $|Q_\perp|$ increasing from 1 to $2+3\tau$.

It can be noticed that the q-basis is taken as relatively large for the parallel bound and small for the perpendicular bound. This is consistent with the experimental diffractions where the observed peaks form an essentially discrete set[1], extending quite far in $|q_\parallel|$ but all with modest $|q_\perp|$ values (typically up the 4-th series in the notations of Cahn *et al.* [22]). As shown, it is crucial to include peaks both with large enough parallel and perpendicular components, especially, high enough series in $q_\perp$ in order to really take into account the quasiperiodicity of the material. Indeed, the right part of the figure 3 shows that a too important truncation in $q_\perp$ leads to a "pendellösung effect" similar to what is observed in usual crystalline aluminum (excitation of two main eigenstates). Increasing the $q_\perp$-basis exalts the quasiperiodic effect.

2.2 *Geometry of the HREM images*

As in crystals, arbitrary orientation of quasicrystals leads to a projection of atoms that fill the image plane and results in an unreadable image. For *rational* orientations, atoms align in columns and the image is a 2D-quasiperiodic pattern of discrete set of dots very similar to HREM images of crystals.

The figure 4-a shows the simulation of a HREM image of the spherical model [18] along the 5-fold $(1,0,0,0,0,0)$ direction. The difficulty in understanding the image lies in the fact that it corresponds to the 2D projection of a 3D-object. For icosahedral structure the proper analysis is in calculating the 4D-projections of a 6D-structural model. To illustrate this purpose, we focus on the two rational directions drawn on fig 4-a, noted A — the 2-fold axis $(0,0,0,1,0,1)$— and noted B —(0,0,1,$\bar{1}$,1,1) in a mirror plane—. They are intersections with $\mathbf{E}_\parallel$ of rational 2D planes in the 6D space as shown on fig 4-b. Each has its own unit cell (see fig 4-c) and projected atomic surfaces. In the case of A, all three kinds (n, n' and bc) of atomic surfaces project at the *same* location. Examination of the HREM image along the A direction shows a (quasiperiodic) sequence of white dots that actually does not distinguish between the three atomic surfaces. For the direction noted B (figure 4-c), the three kinds of the atomic surfaces n, n' and bc project at *different* locations in the unit cell. They are so closely aligned that they form an almost continuous straightline, thus giving the impression of a perfect periodicity of dots along the B direction. This shows that structural interpretation of HREM images should be performed with greatest caution, as an example, drawing a quasicrystalline atomic structure directly on the HREM image with no hyperspace geometrical considerations does not make much sens.

2.3 *The impact of the structural model on the HREM simulation*

[1]High order peaks in perpendicular space are not experimentally observed because of too weak intensities.

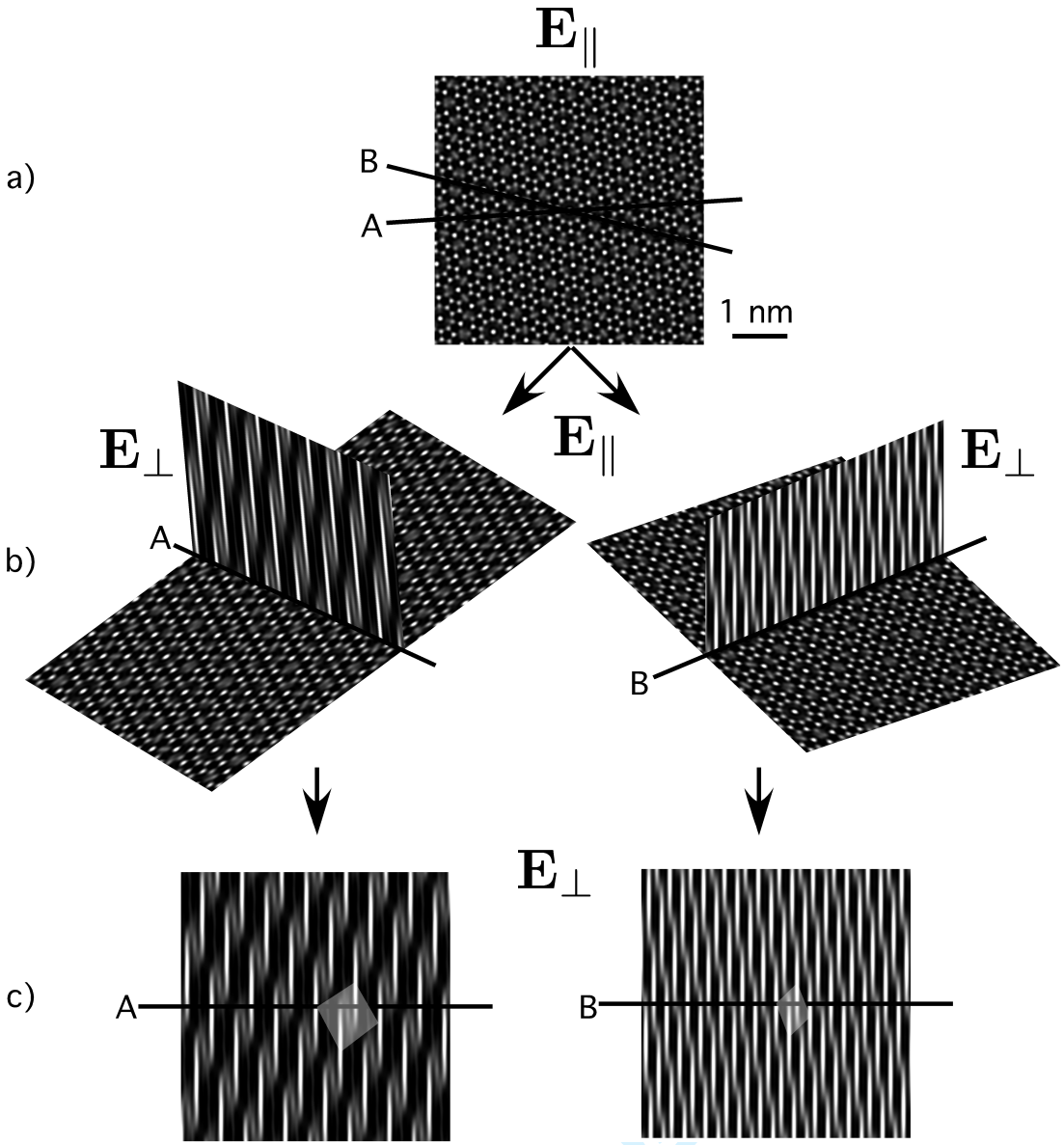

Figure 4. a) Simulation of a HREM image oriented along a 5-fold $(1,0,0,0,0,0)$ axis using the spherical model [18], calculated with 461 beams. The thickness of the foil is $z = 10$ nm with no optical aberrations $\Delta z = 0$ nm, $C_s = C_c = 0$ mm and $\alpha = 0$ mrad. Two different rational orientations noted $A = (0,0,0,1,0,1)$ and $B = (0,0,1,\bar{1},1,1)$ are shown. b) metaphoric view of the 2D rational planes of the 6D space that intersect the HREM simulation plane. c) The 2D rational planes explaining the sequences of dots observed on the image along the directions A and B.

Figure 5 shows two simulations of HREM images built with 171 excited beams, calculated with two different structural models of the same icosahedral phase i-AlPdMn: the spherical model [18] on the left and the polyhedral model [17] on the right. The figure reproduces continuous variations of defocus (from left to right horizontally between -50 and -30 nm) and of thickness (from top to bottom between 0.1 and 20 nm). For thin samples, there are no significant differences between the images: the short atomic distances inherent of the sphere model have no influence on the image both because the image is a projection of the structure and because of course of the limited resolution of the microscope. At thicknesses larger than 10 nm, the images differ enough for a possible differentiation being made.

3 Conclusion

Numerical simulations of quasiperiodic structures are directly possible with no need of an artificial periodicity with a superstructure cell as far as enough beams are introduced in the dynamical calculations

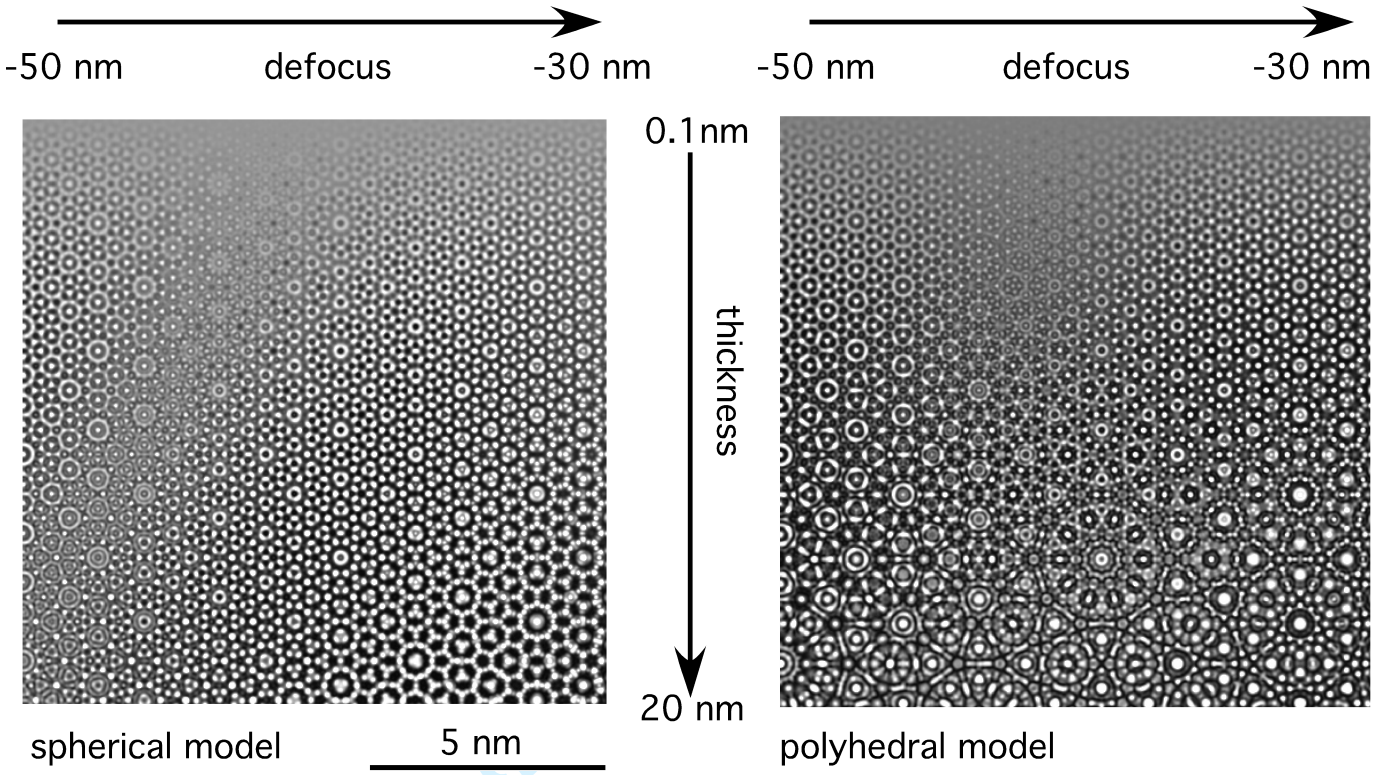

Figure 5. Two simulations of HREM images, both calculated with 171 beams, are presented for different thicknesses of the foil from $z = 0.1$ nm to $z = 20$ nm (vertically on the figure) and for different defocus from $\Delta z = -50$ nm to $\Delta z = -30$ nm (horizontally on the figure). On the left, the calculation describes the atomic structure of the icosahedral phase i-AlPdMn in which the atomic surfaces are spherical [18]. On the right, it is the result of the polyhedral model [17] used to describe the same phase but, in this case, with polyhedral atomic surfaces. In each case, the optical aberration parameters are the same: $C_s = 1$ mm, $\alpha = 0.1$ mrad and $C_c = 4$ mm.

especially those corresponding to high series $q_\perp$ values that are essential for reproducing the main features of the quasiperiodicity of the material, even if they have small diffraction intensities.

HREM images are difficult to use for differentiating various atomic structures: different atomic surfaces can often project at a same localization on the HREM image and the differences in the images, as exemplified on fig 5, appear only for thick enough samples.

However, HREM images are very important for revealing the overall geometry of quasicrystals and thus the possible defects present in these materials such as dislocations. Z-constrast analyses will certainly give new insights for quasicrystal structural determination although the technique is not yet fully understood.

References

[1] D. Shechtman, I. Blech, D. Gratias & J. W. Cahn, Phys. Rev. Lett. **53** 1951-3 (1984).
[2] D. Shechtman & I. Blech, Met. Trans. **16A** 1005 (1985).
[3] R. Portier, D. Shechtman, D. Gratias & J. W. Cahn, J. Microsc. Spectrosc. Electron. Vol **10** n°2 pp.107-116 (1985).
[4] R. Portier, D. Shechtman, D. Gratias & J.Bigot, *Inst. Phys. Conf. Ser.* n° **78** chapter 9 pp. 317-320 (1985).
[5] M. Cornier, R. Portier & D. Gratias, *Inst. Phys. Conf. Ser.* n°**78** chapter 3 pp. 91-94 (1985).
[6] M. Cornier, K. Zhang, R. Portier & D. Gratias, *J. de Phys. Coll. C3* Vol. **47** n°7 pp. 447-456 (1986).
[7] M. Cornier, R. Portier & D. Gratias, *Proc. XIth Int. Cong. on Electron Microscopy*, Kyoto (Japan) pp. 195-198 (1986).
[8] M. Cornier-Quiquandon, *Thèse doctorat de l'Université Paris VI* (1988).
[9] T. Watanabe & Y. Kitano, J. of Electron Microscopy **47(2)**, 129—133 (1998).
[10] W. Yuan-Ming, H. Tian-Bao, W. Huo & Z. Xiaobiao, Phil. Mag. Lett. Vol. **61** n° 1, 29 (1990).
[11] M. V. Berry, J. Phys. C **4**, 697—722 (1971).
[12] M. V. Berry & K. E. Mount, *Rep. Prog. Phys.* **35**, 315—397 (1972).
[13] D. Van Dyck, Phys. Status Solidi **72**, 321—336 (1975).
[14] B. Jap & R. Glaeser, Acta Cryst. **A34**, 94—102 (1978).
[15] D. Gratias & R. Portier, *Inst. Phys. Conf.* Ser. No **61** : Chapter 6 EMAG Cambridge, 275—278 (1981); ibidem 289—292 (1981).
[16] D. Gratias & R. Portier, Acta Cryst. **A39** 576—584 (1983).
[17] M. Quiquandon & D. Gratias, Phys. Rev. **B74**, 214205-1—9 (2006).
[18] M. Boudard, M. de Boissieu, C. Janot, G. Heger, C. Beeli, H.-U. Nissen, H. Vincent, R. Ibberson, M. Audier & J.-M. Dubois, J. Phys. Condens. Matter **4**, 10149 (1992).
[19] D. Gratias, M. Cornier & R. Portier, Acta Cryst. **A44**, 789—798 (1988).
[20] F. A. Lenz, *Electron microscopy in material science* (ed. U. Valdre), Academic Press (London) 539—569 (1971).

[21] F. Thon, *Electron microscopy in material science* (ed. U. Valdre), Academic Press (London) 570—625 (1971).
[22] J. W. Cahn, D. Shechtman & D. Gratias, J. Mater. Res. **1**, 13 (1986).